Baselines for Calculating Crop Water Stress Index in Bean Cultivation

Jane Maria de C. Silveira[1], Juliana de A. Góes[2], Dijaina F. S. Prado[3], Regina Célia de M. Pires[4], Alisson F. Chiorato[5]

[1] Agronomic Institute, IAC, Center for Agricultural Biosystems, Campinas, São Paulo, Brazil – jane.silveira@sp.gov.br
[2] Agronomic Institute, IAC, Center for Agricultural Biosystems, Campinas, São Paulo, Brazil – goes.juliana@outlook.com
[3] University of Paulista, UNIP, Campinas, São Paulo, Brazil – dija-92@hotmail.com
[4] Agronomic Institute, IAC, Center for Agricultural Biosystems, Campinas, São Paulo, Brazil – regina.pires@sp.gov.br
[5] Agronomic Institute, IAC, Grains and Fibers Center, Campinas, São Paulo, Brazil – alisson.chiorato@sp.gov.br

Keywords: CWSI, Modeling, Irrigation, Proximal Sensors, Infrared Radiometer, Canopy Temperature.

Abstract

Efficient irrigation management is vital for conserving water and maximizing productivity, making the crop water stress index (CWSI) a powerful remote sensing tool. CWSI computation requires lower and upper baselines, corresponding to no-stress and severe stress conditions, respectively. This study aims to compare two different methods for determining those baselines. In the empirical method, the non-water-stressed baseline (NWSB) is derived by the linear regression of the canopy-air temperature difference against vapor pressure deficit (VPD) for a well-watered crop. The combined method compares the NWSB coefficients to theoretical expressions to estimate aerodynamic and canopy resistance at potential transpiration. This work used infrared radiometers (IRR) to measure the canopy temperature of bean plants (*Phaseolus vulgaris L.*) cultivar ‘IAC1850’ under center-pivot irrigation. Since the empirical method is susceptible to fluctuations in meteorological data, an expressive amount of data had to be filtered out. When comparing the two methods, the RMSE is 1.0 °C for the lower baseline and 1.8 °C for the upper baseline. Future studies could use these baselines to provide CWSI maps from thermographic images.

1. Introduction

Irrigated agriculture positively affects productivity, improving product supply distribution, reducing production risks associated with the climate, generating employment and income and improving the quality of life. On the other hand, water use in irrigated agriculture is known to impact water abstraction significantly. Therefore, irrigated agriculture is vital in the economic, social and environmental context, as it guarantees food and water security. Due to the increasing demand for food, energy, and goods, coupled with the limited water resources, the need for efficient water management in irrigation is more pressing than ever. It is crucial to manage water for irrigation more efficiently to conserve water and maximize productivity.

Given the current challenges in agriculture, precision irrigation tools must be developed to accurately estimate crop water stress and water use efficiency under deficit irrigation. The crop water stress index (CWSI) is widely used in the remote sensing literature to evaluate deficit irrigation using thermography to obtain the canopy temperature. The CWSI normalizes the difference between the canopy temperature and the air temperature using two boundaries: the lower limit corresponds to a well-watered condition (no stress), and the upper limit relates to no transpiration (severe stress).

These limits are specified by baselines that express the temperature difference as a function of the vapor pressure deficit (VPD). They can be obtained by an empirical method, a theoretical method, or a combination of both. In the empirical method, infrared radiometers (IRR) are typically employed to collect data. Although the empirical method is widely used, it is susceptible to cloud coverage and wind speed. The theoretical method combines energy balance and the Penman-Monteith equation, depending on variables that are difficult to determine, such as aerodynamic resistance. The combined method aims to compensate for the weaknesses of the other two. The purpose of the present study is to compare the empirical and combined methods for determining the lower and upper limits of the CWSI.

2. Materials and Methods

2.1 CWSI Baselines

The CWSI takes values between 0 and 1, with 0 corresponding to no water stress and 1 indicating severe water stress. It is defined by the following expression:

$$\text{CWSI} = \frac{(T_c - T_a) - (T_c - T_a)_{LL}}{(T_c - T_a)_{UL} - (T_c - T_a)_{LL}}, \tag{1}$$

where T_c = canopy temperature
T_a = air temperature
$(T_c - T_a)_{LL}$ = lower limit
$(T_c - T_a)_{UL}$ = upper limit

Although the canopy temperature can be measured with a thermographic camera, the upper and lower limits must be determined using other methods. The following subsections detail three of those methods.

2.1.1 Empirical Method: In the empirical method (Idso et al., 1981), the lower limit $(T_c - T_a)_{LL}$ is given by the linear regression of $(T_c - T_a)$ as a function of the atmospheric VPD and is often referred to as the non-water-stressed baseline (NWSB). The upper limit $(T_c - T_a)_{UL}$ is a constant obtained by extrapolating the NWSB for a negative VPD, which compensates for the residual vapor pressure difference due to $(T_c - T_a)$ at VPD = 0.

$$(T_c - T_a)_{LL} = a + b\ \text{VPD}, \tag{2}$$

$$(T_c - T_a)_{UL} = a + b\ [\text{SVP}(T_a) - \text{SVP}(T_a + a)], \tag{3}$$

where a = intercept of the linear regression
b = slope of the linear regression
VPD = atmospheric vapor pressure deficit
SVP = saturated vapor pressure at a given temperature

2.1.2 Theoretical Method: The theoretical method (Jackson et al., 1981) expresses the temperature difference ($T_c - T_a$) by combining the energy balance and diffusion equations. The lower and upper limits are given by forcing the canopy resistance r_c to zero and infinity, respectively.

$$(T_c - T_a) = \frac{r_a R_n}{\rho C_p}\frac{\gamma(1+r_c/r_a)}{\Delta+\gamma(1+r_c/r_a)} - \frac{\mathrm{VPD}}{\Delta+\gamma(1+r_c/r_a)}, \tag{4}$$

$$(T_c - T_a)_{LL} = \frac{r_a R_n}{\rho C_p}\frac{\gamma}{\Delta+\gamma} - \frac{\mathrm{VPD}}{\Delta+\gamma}, \tag{5}$$

$$(T_c - T_a)_{UL} = \frac{r_a R_n}{\rho C_p}, \tag{6}$$

where r_a = aerodynamic resistance
r_c = canopy resistance
γ = psychrometric constant
R_n = net radiation
C_p = heat capacity of air
ρ = density of air
Δ = slope of the saturated vapor pressure

2.1.3 Combined Method: The theoretical method is prone to inaccuracies when the aerodynamic resistance is not correctly estimated (Han et al., 2018). Moreover, the canopy resistance of a well-watered crop is not null but has a particular value at potential evapotranspiration. The combined method (O'Toole and Real, 1986) solves these issues by comparing equations 2 and 5 and solving for the mean canopy resistance at potential transpiration and the mean aerodynamic resistance. Then, the lower limit is calculated by inserting the mean aerodynamic and canopy resistance (equations 9 and 10) into equation 4. The combined method also considers an infinite canopy resistance for the upper limit (equation 6).

$$a = \frac{r_a R_n}{\rho C_p}\frac{\gamma(1+r_c/r_a)}{\Delta+\gamma(1+r_c/r_a)}, \tag{7}$$

$$b = -\frac{1}{\Delta+\gamma(1+r_c/r_a)}, \tag{8}$$

$$\bar{r}_a = \frac{\rho C_p a}{\bar{R}_n b(\bar{\Delta}+1/b)}, \tag{9}$$

$$\bar{r}_{cp} = -\bar{r}_a\left(\frac{\bar{\Delta}+1/b}{\gamma}+1\right), \tag{10}$$

where $\bar{r}_a$ = mean aerodynamic resistance
$\bar{r}_{cp}$ = mean canopy resistance at potential transpiration
$\bar{R}_n$ = mean net radiation
$\bar{\Delta}$ = mean slope of the saturated vapor pressure

2.2 Experimental Setup

The present study was conducted at the Santa Elisa Experimental Farm at the Agronomic Institute in Campinas, São Paulo, Brazil (22°51'49" South, 47°04'41" West, 656 m altitude). In the experimental area under center-pivot irrigation, beans (*Phaseolus vulgaris L.*) cultivar 'IAC1850' were planted on August 7, 2023, at a planting density of 222,222 plants per hectare. The bean cycle is 91 days long and is divided into five stages of development: vegetative phase, development phase, flowering phase, grain-filling phase and maturation phase.

Throughout the cycle, 12 irrigations were carried out, totaling 131 mm to keep plants well irrigated; there were also 340 mm of recorded precipitation. Table 1 presents the climatic data for each phenological development stage, collected from an automatic station belonging to the Agronomic Institute meteorological network and located approximately 700 meters from the experimental area. The station provided air temperature, precipitation, relative humidity, solar radiation and wind speed data every 20 minutes.

Phenological Phase	Period	Days After Planting	Maximum Temperature (°C)	Minimum Temperature (°C)	Solar Radiation ($MJ.m^{-2}.day^{-1}$)	Wind Speed at 10 m Height ($m.s^{-1}$)
Vegetative	Aug 07 Aug 16	10	29.9	15.8	7.0	0.4
Development	Aug 17 Sep 07	32	28.1	16.8	9.4	2.2
Flowering	Sep 08 Sep 23	61	30.8	19.6	14.9	2.7
Grain Filling	Sep 24 Oct 18	81	30.7	18.9	11.9	2.9
Maturation	Oct 19 Nov 06	91	29.3	19.1	13.8	2.7

Table 1. Average values of maximum and minimum temperatures, average solar radiation and wind speed during the different phenological phases of the bean plant.

Two IRR sensors – model SIL411 from Apogee Instruments – measured the canopy temperature at the experimental area every 5 minutes. Each sensor was installed on August 30 at 0.8 m above the soil surface with a 30° viewing angle, pointing in the east-west planting direction. Because the bean was cultivated with straw mulch and due to the small canopy of the plants in the development phase, the temperature obtained by the IRR sensors showed interference from the straw temperature. Therefore, the lower and upper baselines were determined from September 25 to October 18, 2023, corresponding to the most critical phase for bean production: grain-filling.

3. Results

3.1 Empirical Method

Figure 1 shows the temperature difference as a function of VPD at different hours throughout the day during the grain-filling phase. In the region with VPD higher than 2 kPa, the temperature difference decreases linearly as the VPD increases, from 10h up to 14h. This behavior is explained by the stomata opening during the day to cool the plant until two or three hours before sunset (Idso et al., 1981). Then, from 15h to 17h, VPD decreases, and the temperature difference moves toward a different value than that observed earlier in the day. For VPD below 2 kPa, the data are too scattered due to fluctuations in the net radiation.

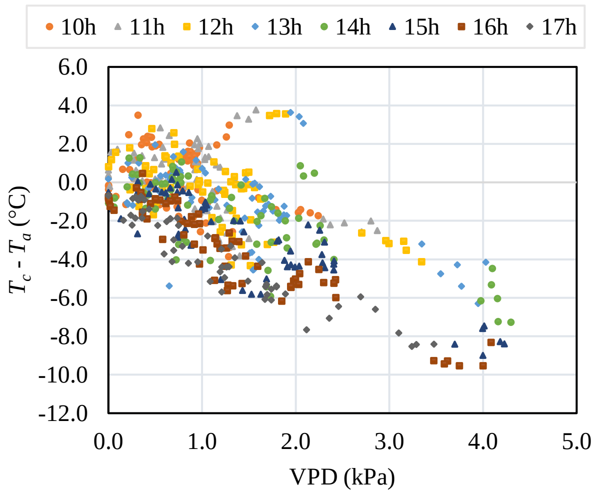

Figure 1. Temperature difference vs. VPD throughout the day during the grain-filling phase.

In Figure 1, a set of outliers makes an arch with higher temperature difference values for VPD between 1.2 and 2.3 kPa. All these points belong to the same day, October 16. That day, air temperature and atmospheric pressure dropped, and air humidity increased, preceding 30 mm of rain in the early hours of the following day. These outlier points were removed to continue the analysis, as seen in Figure 2.

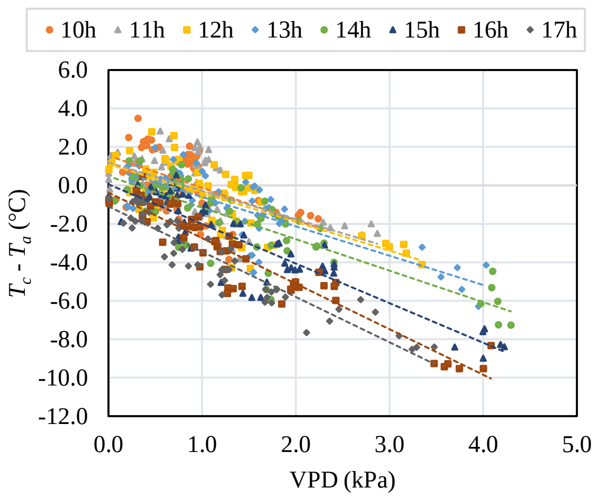

Figure 2. Non-water-stressed baseline (NWSB) throughout the day.

Figure 2 shows the NWSB at different hours. The slope of the linear regressions is nearly constant, while the intercept moves noticeably throughout the day. Table 2 displays the slope standard error, p-value and 95% confidence interval corresponding to each linear regression. Because the confidence intervals intersect, the slope is statistically the same from 10h to 14h. The same occurs between 16h and 17h. This result is consistent with the fact that the slope does not depend on quantities that vary significantly during the day (equation 8).

Time	Slope	Standard Error	p-Value	95% Confidence Interval	
10h	-1.67	0.36	2E-05	-2.39	-0.95
11h	-1.47	0.26	6E-07	-2.00	-0.94
12h	-1.50	0.20	5E-10	-1.91	-1.09
13h	-1.53	0.16	4E-14	-1.84	-1.21
14h	-1.64	0.14	1E-16	-1.93	-1.35
15h	-2.06	0.13	5E-23	-2.32	-1.80
16h	-2.37	0.11	1E-29	-2.59	-2.15
17h	-2.36	0.12	7E-26	-2.60	-2.11

Table 2. Statistics of the slope for the linear regressions at each time.

On the other hand, the intercept moves noticeably throughout the day (see Figure 1). Table 3 shows the statistics for the intercept of each linear regression. Note that the intercept is statistically the same from 10h to 12h but decreases with time in the following hours. This occurs because the intercept is a function of the net radiation (equation 7), which decreases in the afternoon.

Time	Intercept	Standard Error	p-Value	95% Confidence Interval	
10h	1.54	0.34	2E-05	0.87	2.21
11h	1.19	0.30	2E-04	0.59	1.80
12h	1.10	0.28	2E-04	0.55	1.66
13h	0.92	0.25	6E-04	0.41	1.43
14h	0.48	0.25	6E-02	-0.03	0.99
15h	0.06	0.23	8E-01	-0.41	0.52
16h	-0.37	0.19	5E-02	-0.75	0.00
17h	-1.09	0.18	2E-07	-1.45	-0.73

Table 3. Statistics of the intercept for the linear regressions at each time.

The final NWSB (Figure 3) was obtained by selecting data from 10h to 14h, VPD higher than 2 kPa, and wind speed lower than 6 $m.s^{-1}$ at 10 m above the ground level. The resulting slope, intercept and coefficient of determination are -1.92 $°C.kPa^{-1}$, 2.26 °C and 0.78, respectively. Usually, data from cloudy days are disregarded; however, since cloud cover data were unavailable, a VPD threshold was used instead.

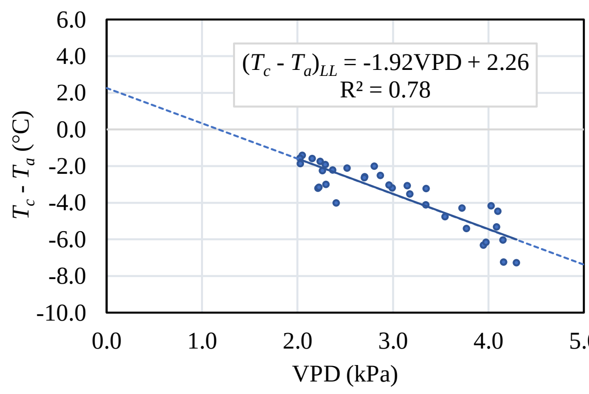

Figure 3. NWSB using data from 10h to 14h.

The last step of the empirical method is to derive the upper baseline from the coefficients of the NWSB (equation 3). As depicted in Figure 4, the resulting temperature difference is not constant but increases slightly with VPD. By performing another linear regression, the ensuing slope, intercept, and coefficient of determination are 0.23 $°C.kPa^{-1}$, 3.01 °C and 0.85, respectively.

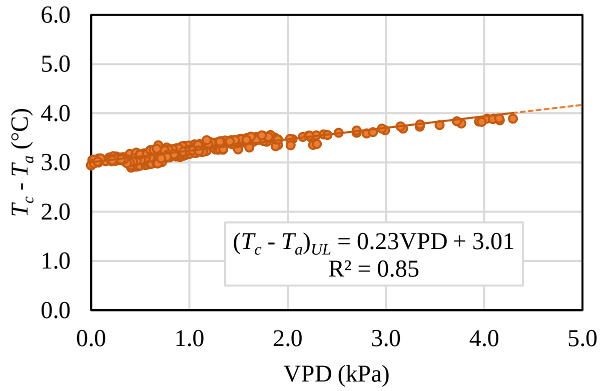

Figure 4. Upper baseline using equation 3.

3.2 Combined method

The combined method estimates the mean aerodynamic and mean canopy resistance at potential transpiration by applying the coefficients from the empirical method to equations 9 and 10. Table 4 indicates all the quantities involved in these calculations. The mean net radiation and slope of the saturated vapor pressure were computed for the days corresponding to the grain-filling phase, from 10h to 14h. The mean air density was derived for the same period, considering the air temperature, atmospheric pressure and relative humidity.

Parameter		Value	Unit
a	NWSB intercept	2.26	°C
b	NWSB slope	-1.92	°C.kPa^{-1}
$\bar{R}_n$	Mean net radiation	329	W.m^{-2}
$\bar{\Delta}$	Mean slope of the saturated vapor pressure	0.22	kPa.°C^{-1}
ρ	Mean air density	1.26	Kg.$^{m-3}$
γ	Psychrometric constant	0.0625	kPa.°C^{-1}
C_p	Heat capacity of air	1000	J.kg^{-1}.°C^{-1}
$\bar{r}_a$	Mean aerodynamic resistance	15.11	s.m^{-1}
$\bar{r}_{cp}$	Mean canopy resistance at potential transpiration	56.43	s.m^{-1}

Table 4. Estimate of the mean aerodynamic and canopy resistances.

If all of these mean values were inserted into equations 4 and 6, then the resulting expression for the lower baseline would be identical to the NWSB from the empirical method, and the upper baseline would be constant, equal to 3.96 °C. However, the net radiation fluctuated considerably during the period in question. Thus, a variable net radiation was used instead. Table 5 indicates the resulting coefficients from computing equations 4 and 6, rewriting them in the following form:

$$(T_c - T_a) = cR_n + d\text{VPD}, \tag{11}$$

Baseline	c (°C.m².W^{-1})	d (°C.kPa^{-1})
Lower	0.0069	-1.92
Upper	0.012	0

Table 5. Coefficients of the combined method (equation 11).

Figure 5 shows the lower and upper baselines, plotting the temperature difference as a function of VPD. For the lower baseline, $d = b$ since only mean values were used to calculate this coefficient. This can be confirmed in Figure 5 for the region where VPD is greater than 2 kPa.

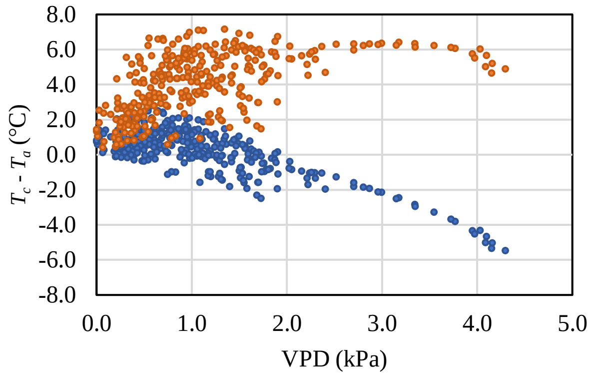

Figure 5. Baselines from the combined method: upper (orange) and lower (blue).

The data seems scattered for VPD lower than 2 kPa as the net radiation varies considerably in that region. However, the difference between the upper and lower limits at each data point is well-behaved, as shown in Figure 6. A linear regression of this data set produces a high coefficient of determination, equal to 0.91. Recall that the difference between upper and lower limits corresponds to the denominator of the CWSI expression (equation 1).

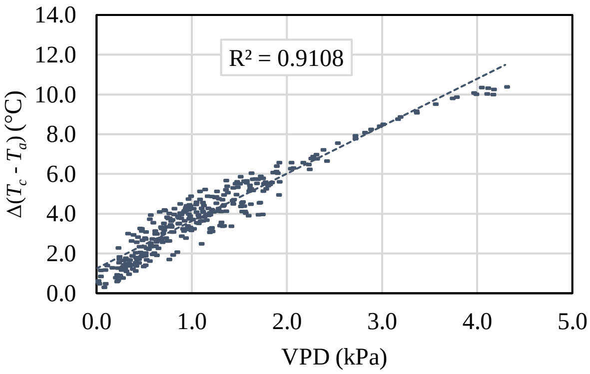

Figure 6. Difference between upper and lower baselines from the combined method.

Moreover, in the combined method, the temperature difference is a function of both the VPD and the net radiation. Indeed, equation 11 can be represented by a plane in a 3D plot, as shown in Figure 7 for the lower limit and Figure 8 for the upper limit. Hence, Figure 5 can be seen as a projection onto a plane of constant net radiation.

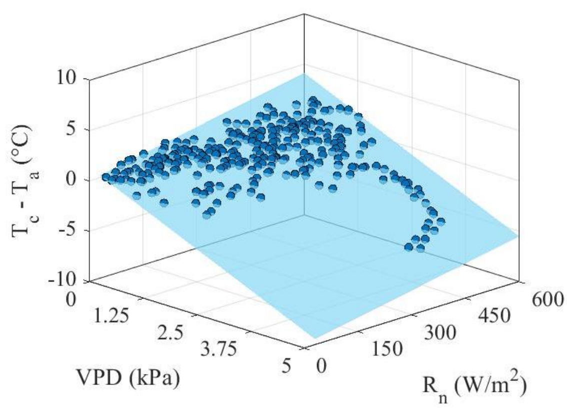

Figure 7. Lower limit of the temperature difference as a function of VPD and net radiation.

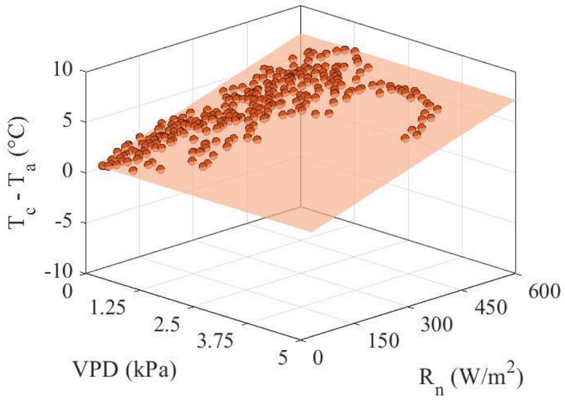

Figure 8. Upper limit of the temperature difference as a function of VPD and net radiation.

3.3 Comparison

The combined method correlates well with the empirical method for the lower limit, as Figure 9 demonstrates. There is a bias when the NWSB (empirical method) is below -2.0 °C, corresponding to VPD greater than 2 kPa. In this region, the combined method temperature difference is, on average, 1.1 °C higher. This bias is explained by the local mean net radiation being higher than the overall mean net radiation, as seen in Figure 7. In contrast, the mean error is 0.1 °C when the NWSB is above -2.0 °C. The resulting root mean square error (RMSE) is 1.0 °C.

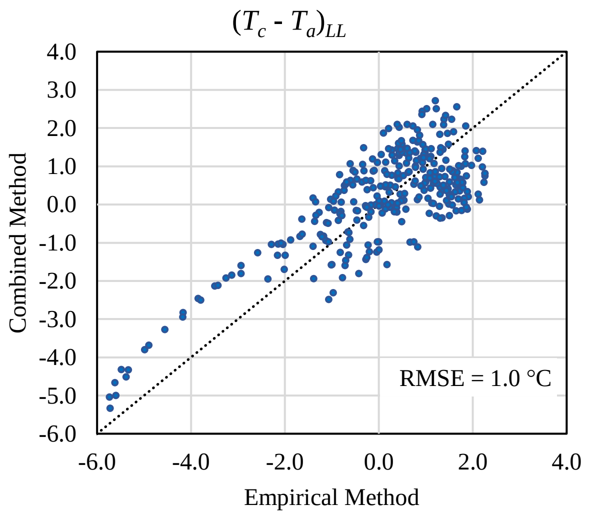

Figure 9. Lower baseline comparison: empirical vs. combined methods. Temperature differences in °C.

For the upper limit (Figure 10), the combined method incorporates more climatic factors, making it more responsive than the empirical method. Also, the combined method produces higher temperature difference values. For VPD greater than 2 kPa, the mean error is 2.2 °C, and for VPD lower than 2 kPa, the mean error is 0.7 °C. The overall RMSE is 1.8°C.

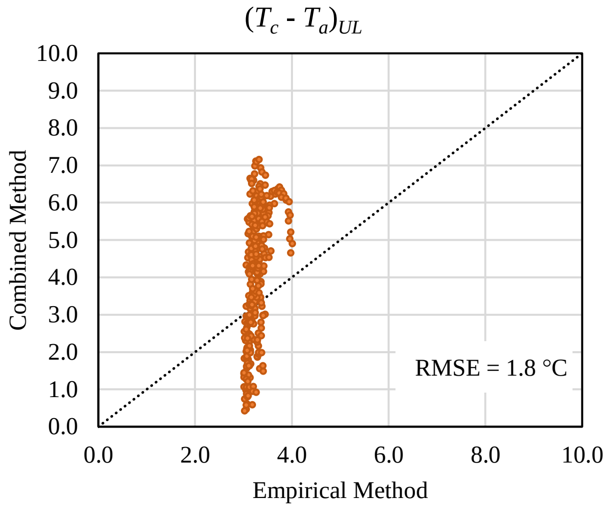

Figure 10. Upper baseline comparison: empirical vs. combined methods. Temperature differences in °C.

4. Discussion

The empirical method is known to be susceptive to net radiation and wind speed fluctuations (Jackson et al., 1988). Usually, only data from clear and sunny days are considered, and a wind speed threshold is also applied to filter the data (Bellvert et al., 2016; Gonzalez-Dugo et al., 2014; Katimbo et al., 2022). However, this work used a VPD threshold in addition to limiting the wind speed because cloud coverage data was not available. Though this method produced good results, a lot of data was filtered out.

The NWSB behavior at different times was similar to the one observed by Testi et al., 2008. In Figure 2, the intercept remained statistically constant from late morning to noon, then reduced in the afternoon. In their case, however, the intercept increased from morning until noon and also decreased in the afternoon.

As for the combined method, the estimated values of mean aerodynamic resistance and mean canopy resistance obtained with the combined method are consistent with the literature (O'Toole and Real, 1986). Also, according to Han et al., 2018, the CWSI obtained with this method is less sensitive to variations in the linear regression coefficients (equation 2). The most likely reason is that the combined method introduces another dimension to the model, making the temperature difference a function of both the net radiation and the VPD (see Figure 7 and Figure 8).

Although that is also true for the theoretical model, that model is unreliable (Han et al., 2018). The main difficulty is estimating the aerodynamic resistance (Jackson et al., 1988).

5. Conclusions

The CWSI is a valuable tool for irrigation management. Since canopy temperature can be measured with thermography, it can also be used in remote sensing. However, this index requires an upper and a lower baseline to be calculated. This work compares two different methods of obtaining these baselines. The empirical method is based on a simple linear regression. Still, its greatest drawback is that a significant amount of data must be filtered out because it does not consider the net radiation. The combined method requires additional information, but it adds another dimension to the model that contemplates changes in net radiation. When comparing the two methods, the RMSE is 1.0 °C for the lower baseline and 1.8 °C for the upper baseline.

https://doi.org/10.5194/isprs-archives-XLVIII-3-2024-501-2024 | © Author(s) 2024. CC BY 4.0 License.

For both methods, the first step is to obtain the NWSB – the empirical lower baseline, which expresses the canopy-air temperature difference as a function of VPD in a no-water-stress scenario. In this work, IRR sensors were used to measure the canopy temperature. These sensors allow the measurement of the radiation flow from the plant canopy without physical contact with the leaves and enable up-to-date data storage. The selected data for deriving the NWSB comprised the 10h to 14h period, VPD lower than 2 kPa and wind speed lower than 6 $m.s^{-1}$.

This work contemplates data from a bean crop (*Phaseolus vulgaris L.*) cultivar ‘IAC1850’ under center-pivot irrigation. Although it only analyses data from the grain-filling phase, other phenological phases shall be investigated shortly. Then, at a future time, CWSI maps shall be derived from thermographic images.

Acknowledgments

This work was financed in part by the Agricultural Research Support Foundation (FUNDAG); the National Council for Scientific and Technological Development (CNPq), PIBIC 136722/2023-7; and the São Paulo Research Foundation (FAPESP), CCD 2021/11762-5 and CCD 2022/09319-9.

References

Bellvert, J., Marsal, J., Girona, J., Gonzalez-Dugo, V., Fereres, E., Ustin, S.L., Zarco-Tejada, P.J., 2016. Airborne Thermal Imagery to Detect the Seasonal Evolution of Crop Water Status in Peach, Nectarine and Saturn Peach Orchards. Remote Sensing 8, 39. https://doi.org/10.3390/rs8010039

Gonzalez-Dugo, V., Zarco-Tejada, P.J., Fereres, E., 2014. Applicability and limitations of using the crop water stress index as an indicator of water deficits in citrus orchards. Agricultural and Forest Meteorology 198–199, 94–104. https://doi.org/10.1016/j.agrformet.2014.08.003

Han, M., Zhang, H., DeJonge, K.C., Comas, L.H., Gleason, S., 2018. Comparison of three crop water stress index models with sap flow measurements in maize. Agricultural Water Management 203, 366–375. https://doi.org/10.1016/j.agwat.2018.02.030

Idso, S.B., Jackson, R.D., Pinter, P.J., Reginato, R.J., Hatfield, J.L., 1981. Normalizing the stress-degree-day parameter for environmental variability. Agricultural Meteorology 24, 45–55. https://doi.org/10.1016/0002-1571(81)90032-7

Jackson, R.D., Idso, S.B., Reginato, R.J., Pinter Jr., P.J., 1981. Canopy temperature as a crop water stress indicator. Water Resources Research 17, 1133–1138. https://doi.org/10.1029/WR017i004p01133

Jackson, R.D., Kustas, W.P., Choudhury, B.J., 1988. A reexamination of the crop water stress index. Irrig Sci 9, 309–317. https://doi.org/10.1007/BF00296705

Katimbo, A., Rudnick, D.R., DeJonge, K.C., Lo, T.H., Qiao, X., Franz, T.E., Nakabuye, H.N., Duan, J., 2022. Crop water stress index computation approaches and their sensitivity to soil water dynamics. Agricultural Water Management 266, 107575. https://doi.org/10.1016/j.agwat.2022.107575

O’Toole, J.C., Real, J.G., 1986. Estimation of Aerodynamic and Crop Resistances from Canopy Temperature1. Agronomy Journal 78, 305–310. https://doi.org/10.2134/agronj1986.00021962007800020019x

Testi, L., Goldhamer, D.A., Iniesta, F., Salinas, M., 2008. Crop water stress index is a sensitive water stress indicator in pistachio trees. Irrig Sci 26, 395–405. https://doi.org/10.1007/s00271-008-0104-5